NUMERICAL SIMULATIONS OF LARGE EDDIES IN THE COMPRESSIBLE MIXING-LAYER

F. Ramella*

Politecnico di Torino, Dipartimento di Ingegneria Aeronautica e Spaziale
Torino, Italy

Abstract

In this paper numerical simulation of compressible free shear layers in open domain is performed. Forced temporally-growing mixing-layers are studied. Details of vortex roll-up, pairing and nutation processes are presented. The effect of intrinsic compressibility on the evolution of the large scale vortical structures which develop from primary instability is identified and discussed. As the compressibility parameter we use the convective Mach number M_c defined as the ratio of the velocity difference to the sum of the free stream sound speeds. An explanation of the compressibility stabilizing effect follows from the analysis of the (inviscid) equation which describes the rate of change of the vorticity. The relative magnitude of the term which represents the change due to the compression of fluid elements, and which causes an opposite concentration with respect to the advection (incompressible) mechanism, is evaluated and discussed. The effect of the baroclinic term due to the unequal free stream mean temperature is also illustrated.

Introduction

A massive attention has been recently paid to the study of the compressibility effects in the plane mixing-layer, the prototype of free-shear flows. It is a particularly attractive area of study either for theoretical investigations on the interactions between characteristic dynamical events with coherent history over substantial times (the so-called organized or coherent structures), or for practical development of propulsion systems based on supersonic combustion. A number of laboratory experiments and numerical simulations have showed a strong reduction in the mixing-layer growth rate $d\delta/dx$ (where δ is a convenable measure of mixing-layer width and x is the streamwise coordinate) as the Mach number is increased. Consequently the mixing capability of the shear layer is strongly reduced. Brown and Roshko [1] noted that while the density ratio of the two streams had a noticeable effect on the spreading rate of the mixing layer, it was not enough to explain the slow spreading rate of supersonic mixing layers. Papamoschou and Roshko [2] showed that this compressibility effect could be parameterized in terms of a single Mach number, the Convective Mach Number M_c defined by $M_c = (U_1 - U_2)/(a_1 + a_2)$ where U_1 and U_2 are the free stream velocities and a_1, a_2 are the free stream sound speeds.
Recent experiments [3], stability analyses [4] and numerical simulations [5,6,7,8] have provided further support to this notion.

In this paper we will study the nonlinear evolution of two-dimensional instability waves in the unbounded mixing-layer. The aim is to describe the rilevant effects of compressibility on large-scale structures which develop from the primary inflexional (inviscid) instability of the mean flow. In this stage of instability the most unstable wave is two-dimensional. The well-known sensitivity of the shear layer to its initial conditions implies the possibility of controlling its development by means of external forcing. The goal of this external control is to enhance the spread rate of the layer and, hence, the mixing between the two streams. Then we will investigate the evolution of a forced shear flow. The temporal approximation that we have adopted corresponds to a simulation of the flow by employing a Galilean space-time transformation to concentrate on a small section of the flow field that moves with the flow average velocity. This leads to neglet locally the spatial spreading of the layer and impairs the comparison with experimental results. Motivation behind this approach is offered by the computational savings inherent in the small size of the computational domain. A direct consequence of this approach is the implementation of periodic boundary conditions in the streamwise flow direction.

Mixing-layer flows

Mixing processes are created by the merging, downstream of a splitter plate or a bluff body, of two

*PhD Student

parallel streams flowing with unequal speed. The two streams match in static pressure but, in general, have different fluid densities. Experimental evidence suggests that the flow field resulting from this merging is essentially two dimensional at its early stages and is dominated by large vortical structures (eddies). These structures form as a result of the inherent instability of the velocity profile between the two layers and represent the primary mechanism of entrainment. The development of the layer follows the amplification of perturbations via the Kelvin-Helmholtz instability, which, in its nonlinear stage, leads to roll-up and the formation of concentrated vortices. Further development is dominated by the mutual interactions of these vortices. These interactions, which are a manifestation of the growth of the subharmonic mode of instability, lead to the formation of larger vortical structures and are, hence, the prime contributors to the growth of the layer.

Governing equations

Unsteady two-dimensional compressible viscous flows are described by the full Navier-Stokes system. In compact vectorial formulation it can be written as:

$$\frac{\partial Q}{\partial t}+\frac{\partial F}{\partial x}+\frac{\partial G}{\partial y}=\frac{1}{Re}\left(\frac{\partial F_v}{\partial x}+\frac{\partial G_v}{\partial y}\right) \quad , \qquad (1)$$

where Q is the vector of conservative variables $Q=(\rho,\rho u,\rho v,E)^T$, F and G are the convective fluxes defined as

$$F=\begin{pmatrix}\rho u\\ \rho u^2+p\\ \rho uv\\ (E+p)u\end{pmatrix} \quad , \quad G=\begin{pmatrix}\rho v\\ \rho uv\\ \rho v^2+p\\ (E+p)v\end{pmatrix} \quad ;$$

and F_v and G_v are the viscous terms

$$F_v=\begin{pmatrix}0\\ \tau_{xx}\\ \tau_{xy}\\ u\tau_{xx}+v\tau_{xy}+\frac{\mu}{(\gamma-1)Pr}\frac{\partial a^2}{\partial x}\end{pmatrix} \quad ,$$

$$G_v=\begin{pmatrix}0\\ \tau_{xy}\\ \tau_{yy}\\ u\tau_{xy}+v\tau_{yy}+\frac{\mu}{(\gamma-1)Pr}\frac{\partial a^2}{\partial y}\end{pmatrix} \quad .$$

All the quantities in the equations are dimensionless. As reference values for this normalization we use the upper free stream physical quantities:

$$\rho=\frac{\rho^*}{\rho_{\infty 1}} \quad , \quad u=\frac{u^*}{a_{\infty 1}} \quad , \quad v=\frac{v^*}{a_{\infty 1}} \quad , \quad E=\frac{E^*}{\rho_{\infty 1}a_{\infty 1}^2} \quad ,$$

where $a^2=\gamma p/\rho$ is the speed of sound. The superscript $(*)$ refers to dimensional quantities, the subscript (1) refers to the upper ($y \geq 0$, say faster) free stream, and the subscript (2) to the lower free stream. The reference lengthscale for the specific problem is the vorticity thickness $\delta^*_{w_0}$ of the initial velocity profile:

$$\delta^*_{w_0}=\frac{U_1^*-U_2^*}{\mid \mathrm{d}\bar{u}_0^*/\mathrm{d}y^* \mid_{\max}} \quad , \qquad (2)$$

where $\bar{u}_0$ is the specified initial mean velocity profile. The characteristic associated time is given by: $t=t^* a_{\infty 1}/\delta^*_{w_0}$. The Reynolds number in equations (1) is correlated to the Reynolds number based on the free stream velocity $u_{\infty 1}$ by means of the Mach number $M_{\infty 1}=u_{\infty 1}/a_{\infty 1}$:

$$Re=\frac{\rho_{\infty 1}\delta^*_{w_0}a_{\infty 1}}{\mu_{\infty 1}}=\frac{1}{M_{\infty 1}}\frac{\rho_{\infty 1}\delta^*_{w_0}u_{\infty 1}}{\mu_{\infty 1}} \quad .$$

The non-dimensional costitutive relations for the Newtonian fluid are:

$$\begin{aligned}\tau_{xx} &= \frac{\mu}{3}\left(4\frac{\partial u}{\partial x}-2\frac{\partial v}{\partial y}\right)\\ \tau_{xy} &= \mu\left(\frac{\partial u}{\partial y}+\frac{\partial v}{\partial x}\right)\\ \tau_{yy} &= \frac{\mu}{3}\left(-2\frac{\partial u}{\partial x}+4\frac{\partial v}{\partial y}\right)\end{aligned}$$

The perfect-gas law in our non-dimensional scheme is

$$p=(\gamma-1)\left(E-\rho\frac{u^2+v^2}{2}\right) \quad ; \qquad (3)$$

the viscosity μ is assumed to follow the Sutherland law, and the specific-heat ratio γ is equal to 1.4. In all the simulations we take the Prandtl number to be constant, i.e. $Pr=1$.

Numerical method

A two-dimensional code [9] was used for these simulations. Navier-Stokes equations are resolved in their entirety, with no turbulence model, by using a conservative finite-differences technique, for a compressible viscous flow which grows in time. Advance in time is performed by means of fourth-order explicit Runge-Kutta integration scheme. To simulate an infinite domain in the non-periodic y-direction, characteristic non-reflecting boundary conditions [10] are imposed. The boundaries are collocated sufficiently away from the viscous shear layer so that characteristic form of Euler equations can be considered. Outgoing characteristics use informations

from within the computational domain, and hence any manipulations are requested. Incoming characteristics are handled by setting the time-derivative of their amplitude equal to zero, thus giving the boundary conditions their non-reflecting character.

Convective fluxes are evaluated by using a second-order upwind flux-splitting scheme. The adopted scheme is an improved Advection Upwind Splitting Method (AUSM) proposed by Wada & Liou [11]. This scheme combines the procedure of resolving an approximate Riemann problem at the interfaces (Flux Difference Splitting approach) with the procedure of splitting into travelling components (Flux Vector Splitting approach). Its main property is that it removes the large numerical dissipation on contact discontinuities and shear layers which was the main drawback of classical flux-vector schemes. In particular, it can reproduce with no numerical dissipation the exact Riemann solution for stationary or moving contact discontinuities. Its adoption is justified also by its shock-capturing property: in fact, as we will show in a later section, weak shock waves develop in the flow field for a convective Mach number approximately above 0.7.

Viscous terms are evaluated by using a standard second-order centred scheme.

In the temporally evolving simulations the initial conditions provide the source of disturbances. A base flow is assumed to be described by a velocity profile $\bar{u}_0(y)$, a temperature profile $\bar{T}_0(y)$ and by a constant thermodynamic pressure. The specific base velocity profile we use is the one which would be brought about by molecular diffusion from initial coplanar discontinuity of horizontal velocity at $y = 0$, i.e. the error function:

$$\bar{u}_0(y) = \text{erf}\left(\frac{y^*\sqrt{\pi}}{\delta^*_{w_0}}\right) \quad . \tag{4}$$

The initial mean temperature profile is specified as a solution of the compressible boundary-layer energy equation. For the antisymmetric mean velocity profile, with equal free stream temperatures ($T2/T1 = 1$) the Crocco-Busemann solution is given by:

$$\bar{T}_0(y) = 1 + M_1^2\frac{\gamma-1}{2}(1-\bar{u}_0^2) \quad . \tag{5}$$

Small amplitude disturbances are then added to the mean flow. All the perturbations have the form

$$\psi_0(x,y) = \sum_{\kappa=1,\frac{1}{2},\frac{1}{4},\ldots} a^0_\kappa \frac{1}{2}\left[\hat{\psi}_\kappa(y)e^{i(\kappa\alpha x-\phi_{0\kappa})} + c.c.\right]$$

where $c.c.$ denotes the complex coniugate. The distributions $\hat{\psi}_\kappa$ are the stability eigenfunctions presented in the next section. The phase ϕ_{01} is irrelevant to the evolution of the flow, and is set to π for convenience (the Kelvin's cat's-eye, the characteristic closed recirculating region, is centred on the computational box). The amplitude a^0_1 for the fundamental mode was selected with a relative magnitude of 5% with respect to the largest normalized perturbation component. The relative ratio of the amplitude of subsequent subharmonics $a^0_{\kappa/2}/a^0_\kappa$ was selected equal to 0.5. The phases $\phi_{0\kappa}$ of the subharmonics ($\kappa = \frac{1}{2}, \frac{1}{4}, \ldots$) relative to the fundamental ($\kappa = 1$) determine whether large-scale amalgamations occur by pairing or shredding. In most cases the optimum pairing phase ($\phi_{0\kappa} = \pi$) was selected. The inibition of the corotation and subsequent pairing amalgamation by shredding interaction between the Kelvin's rollers was indagated by varing the phase $\phi_{0\frac{1}{2}}$ from π to the critical shredding angle $\phi_{0\frac{1}{2}} = 0$ (these results will be discussed in a later section and illustrated in the figure (5a)). The temporal approximation, as discussed above, yields to perform the simulations on a small section of the flow field that moves with the mean velocity $(U_1+U_2)/2$. The streamwise length of this (rectangular) domain is fixed to accomodate the largest wavelength of the perturbations. The bulk of our simulations with composite initial perturbations was performed with initial disturbances which include only the most unstable mode from linear theory and its first subharmonic. All the computations were conducted at a Reynolds number based on initial vorticity thickness and free-stream velocity of 400, which was sufficiently low to resolve the flow fully by adopting a computational mesh with 151 by 151 grid points in the streamwise (uniform mesh) and trasversal direction (with clustering of points in the shearing region) when the domain contains two wavelengths of the most unstable disturbances, and 255 by 181 grid points for initial disturbances which include also the second subharmonic.

Linear stability analysis

Linear stability analysis [12] is employed to reproduce the modification of the early stages of the instability of the vorticity layer. The dependent variables are splitted into base and perturbation components. The perturbation components are assumed to exhibit the form of propagating waves:

$$(u', v', \rho', T', p') = (\hat{u}, \hat{v}, \hat{\rho}, \hat{T}, \hat{p})\exp[i\alpha(x-ct)]$$

where α is the wavenumber, c is the wave speed and $\omega = \alpha c$ is the frequency. Since temporal instabili-

ties are considered in the present work, α is real and $\omega = \alpha c_r + i\alpha c_i$ is complex. The imaginary and real part of ω represent the temporal growth rate and the frequency of oscillation of the disturbances, respectively. Disturbances are amplified when c_i is positive, damped when c_i is negative, and are neutrally stable when c_i is zero. The perturbed quantities are introduced into the compressible Navier-Stokes equations. Since inviscid compressible free shear flows are more unstable than viscous ones because of the existence of inflexional point in the velocity profile, the molecular diffusion is neglected. Linearization is then performed by neglecting, as small, terms involving the products of the perturbations. We obtain the following equations for the disturbance amplitudes:

$$i(\alpha\bar{u} - \omega)\hat{\rho} + \bar{\rho}i\alpha\hat{u} + \hat{v}\frac{\mathrm{D}\bar{\rho}}{\mathrm{D}y} + \bar{\rho}\frac{\mathrm{D}\hat{v}}{\mathrm{D}y} = 0 \quad ;$$

$$i\bar{\rho}(\alpha\bar{u} - \omega)\hat{u} + \bar{\rho}\frac{\mathrm{D}\bar{u}}{\mathrm{D}y}\hat{v} = -\frac{i\alpha}{\gamma M_1^2}\hat{p} \quad ;$$

$$i\bar{\rho}(\alpha\bar{u} - \omega)\hat{v} - \frac{i\alpha}{\gamma M_1^2}\frac{\mathrm{D}\hat{p}}{\mathrm{D}y} \quad ;$$

$$\bar{\rho}[i(\alpha\bar{u} - \omega)\hat{T} + \hat{v}\frac{\mathrm{D}\bar{T}}{\mathrm{D}y}] = -(\gamma - 1)\bar{p}[i\alpha\hat{u} + \frac{\mathrm{D}\hat{v}}{\mathrm{D}y}] \quad .$$

The pressure disturbance $\hat{p}$ is obtained from the perfect gas equation of state:

$$\hat{p} = \bar{\rho}\hat{T} + \hat{\rho}\bar{T} \quad .$$

By employing a process of elimination, an equation governing the evolution of one cross-stream perturbation variation is obtained. In our work, this perturbation is chosen to be the cross-stream velocity, i.e. $\hat{v}$, so that:

$$\frac{\alpha^2(\bar{u}(y) - c)}{\bar{T}(y)}\hat{\phi} = \frac{\mathrm{D}}{\mathrm{D}y}\left[\frac{(\bar{u}(y) - c)\frac{\mathrm{D}\hat{\phi}}{\mathrm{D}y} - \frac{\mathrm{D}\bar{u}(y)}{\mathrm{D}y}\hat{\phi}}{\bar{T}(y) - M_1^2(\bar{u}(y) - c)^2}\right] \quad ,$$

where $\hat{\phi} = i/\alpha\hat{v}$. Its solution poses an eigenvalue problem due to the presence of the wave parameters, α and c. The boundary conditions are imposed by considering that away from the initial interface between the parallel streams all the perturbations decay to zero. Our solutions were obtained by treating the complex wave speed c as an eigenvalue for an externally specified real wave number α by using a direct spectral collocation (pseudospectral) method based on series expansion in term of Chebyshev orthogonal polynomials [13]. The eigenfunctions are normalized so that the real part of the trasversal velocity perturbation $\hat{v}$ is symmetric in y (and positive at $y = 0$), its imaginary part is antisymmetric, and the perturbation energy integrated across the layer is one.

Results from the above analysis are plotted in the figure (1) which show the temporal amplification rate αc_i versus the wave number α for different Convective Mach numbers (for the same temperature ratio $T_2/T_1 = 1.$) The figure clearly shows that the growth factor of the most unstable mode of the Kelvin-Helmholtz instability is strongly reduced as M_c is increased. Experimental results, as well as the results of our numerical simulations presented in the next sections, indicate that this type of behavior persists into nonlinear stages of the evolution.

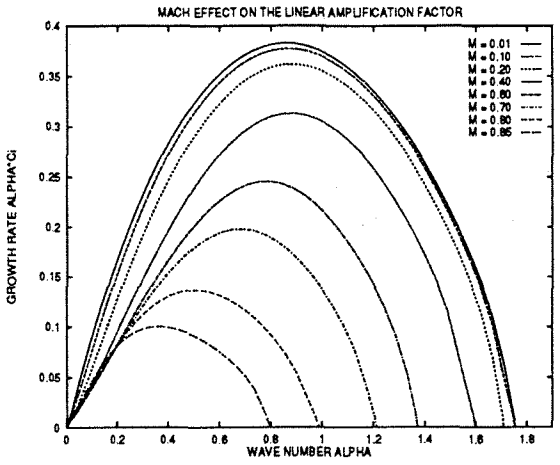

Figure 1: Linear stability analysis results: effect of Mach number on the growth of two-dimensional waves (T2/T1=1.0)

Two-dimensional pairings

The temporal evolution of the two-dimensional instability can be easily described in terms of redistribution in space of the vorticity that the layer possesses initially. During the first stage (Kelvin-Helmholtz roll-up) a concentration of vorticity appears into periodically spaced region (the cores) joined by thin layers (the braids) in which the vorticity is also concentrated. The thin layers are the channels along which vorticity is advected into the cores, and the cores provide the strain which creates the braids. Further in time, pairs of well-developed rollers come together, corotate and eventually amalgamate (pairing process). Both the number of rollers and the number of braid region are thus halved, with the contents of every other braid region being absorbed into the new paired roller. The surviving braid

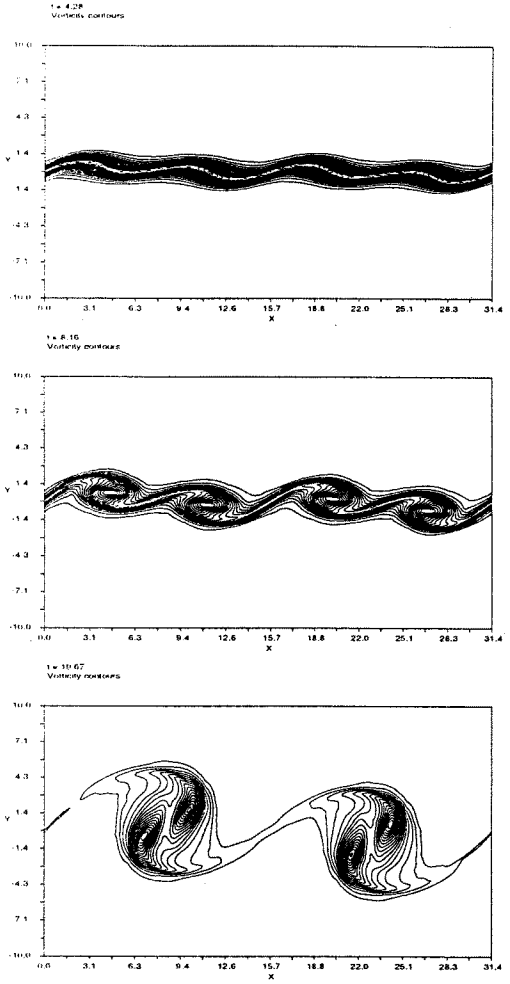

Figure 2: Contours of constant vorticity during the roll-up and the first pairing events; $M_c = 0.4$, $\alpha = 0.85$, $a_1^0 = .05$, $a_{1/2}^0 = .025$, $a_{1/4}^0 = .0125$, $Re = 400$

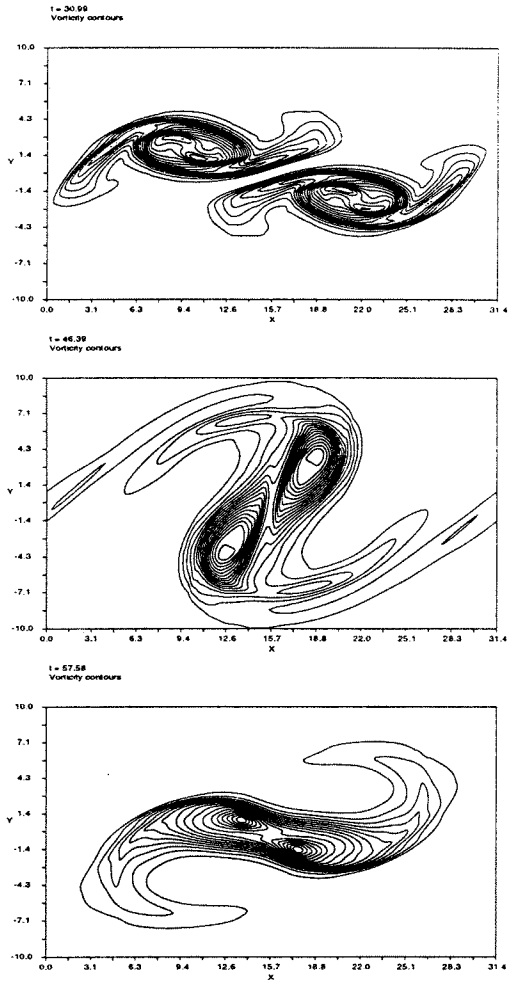

Figure 3: Contours of constant vorticity during the second pairing event; $M_c = 0.4$, $\alpha = 0.85$, $a_1^0 = .05$, $a_{1/2}^0 = .025$, $a_{1/4}^0 = .0125$, $Re = 400$.

region continues to be depleted of spanwise vorticity as all the vortical fluid is drawn into the paired roller. As the cores of the original spanwise rollers merge into a new, roughly circular, core, spiral arms of weaker spanwise vorticity are ejected away form the paired eddy. This process repeats itself after each pairing as we can see in the temporal sequence illustrated in figures (2-3) that show the vorticity redistribution for a simulation with $M_c = 0.4$ and two-subharmonics added to the fundamental mode. As a pairing proceeds, the thickness of the layer (as measured by the area of the Kelvin's cat's-eye, see figure (4)) and the streamwise lengthscale double. Since the velocity scale remains the same, the timescale also doubles and the time between pairing approximately also doubles. For the same reason the strain rate in the surviving mid-braid region is approximately halved with each pairing (as it can be seen in figure (5b)). When only the fundamental mode is superimposed to the mean flow (single roll-up case, illustated in figure (4)) the roller cores become elliptical, the spanwise vorticity is advected into the braid region (oversaturation), and the vortices continue to undergo shape oscillations for several cycles (nutation process). In the pairing cases, the corotation of pairs of rollers begins in most cases before oversaturation occurs. The occurrence or suppression of an oversaturation before a pairing depends on the relative amplitude and phase between the subsequent subharmonics (as it can be seen in figure (5a)). The re-entry of spanwise vorticity into the braid region after the pairing (or before, if the pairing is delayed) can be deduced by observing the evolution of the vorticity contents $-\omega_b$ in the mid-braid plane. This re-entry is marked by sudden increases in the evolution of $-\omega_b$ (figure (5a)).

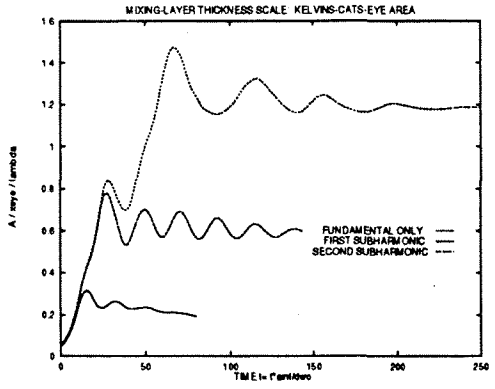

Figure 4: The growth rate of cat's-eye area for different contents of subharmonics into the initial external forcing; $M_c = 0.4$, $Re = 400$, $\alpha = 0.85$, $a_1^0 = .05$, $a_{1/2}^0 = .025$, $a_{1/4}^0 = .0125$

When surviving paired rollers do not undergo further pairings, one can observe a final re-entry which indicates that the nutation process begins.

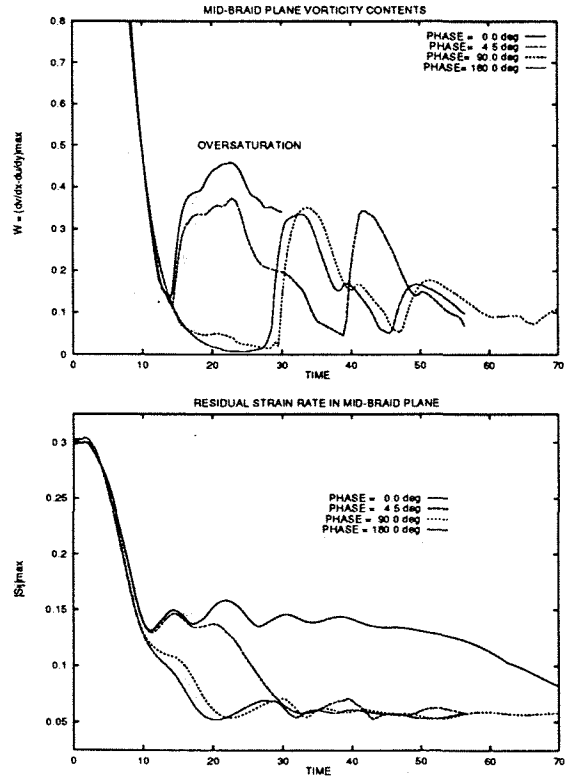

Figure 5: Vorticity contents (top) and residual strain rate (botton) in surviving mid-braid plane for different phase angles between the fundamental mode and its first subharmonic; $M_c = 0.4$, $Re = 400$, $\alpha = 0.85$.

Compressibility effects

Experiments have documented the reduction in the growth rate of compressible shear layers as M_c is increased. In figure (6) we show the time history of the vorticity thickness $\delta_w(t)$, defined as:

$$\delta_w(t) = \frac{2u_{\infty 1}}{\mid d\bar{u}/dy \mid_{max}} \quad , \tag{6}$$

for different M_c.

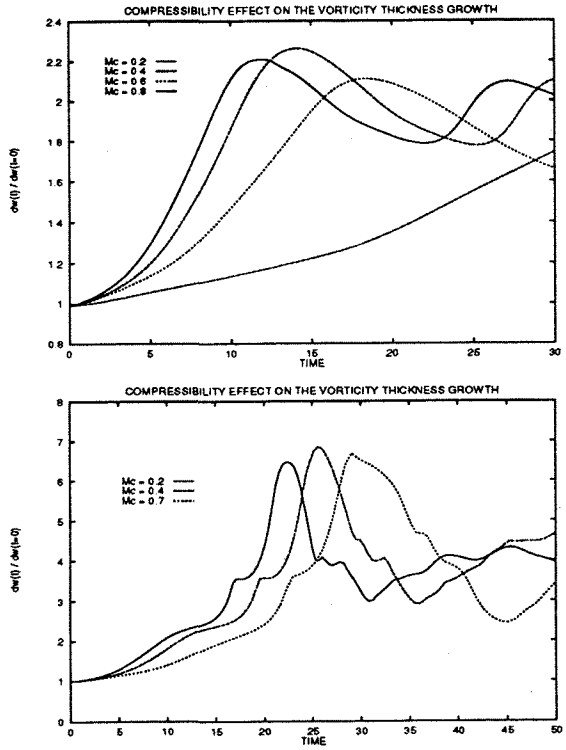

Figure 6: Compressibily effect on the vorticity thickness growth: fundamental mode only (top) and with its first subharmonic included (botton).

The stabilizing influence of M_c is clearly seen. This slow growth arises primarily because of the reduced linear instability growth rate. A physical argument for this stabilizing effect [15] in the nonlinear stages of the evolution follows from the analysis of the inviscid vorticity equation, which describes the rate of change of vorticity with respect to a moving reference frame:

$$\begin{aligned} \omega_z(x,y) &= \frac{\partial v}{\partial x} - \frac{\partial u}{\partial y} \quad , \\ \frac{\partial \omega_z}{\partial t} + U_c \frac{\partial \omega_z}{\partial x} &= -(u - U_c)\frac{\partial \omega_z}{\partial x} - v\frac{\partial \omega_z}{\partial y} \\ & \quad -\omega_z \vec{\nabla} \cdot \vec{u} + \frac{\vec{\nabla}\rho \times \vec{\nabla} p}{\rho^2} \quad , \end{aligned} \tag{7}$$

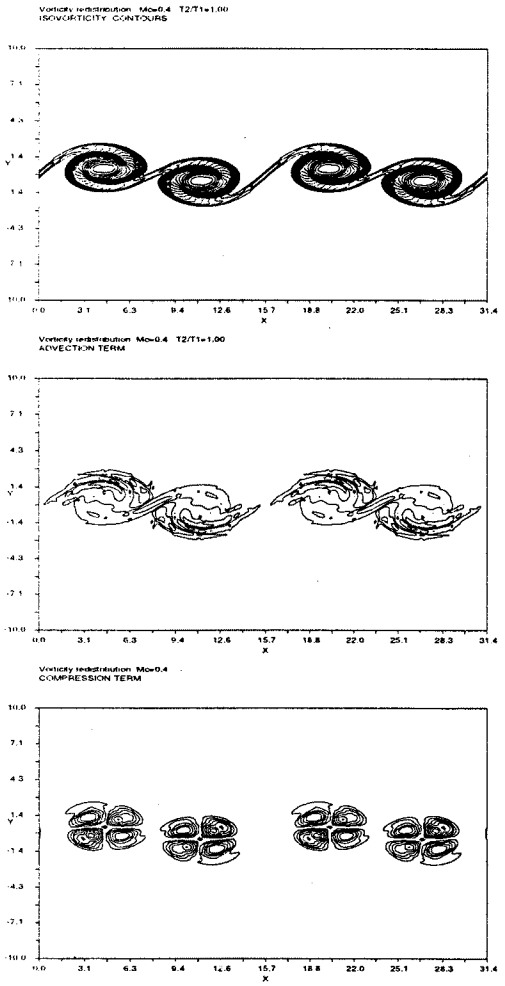

Figure 7: Vorticity field redistribution for $M_c = 0.4$ ($T2/T1 = 1.$). In the panels are illustrated: (a) Vorticity isocontours [-0.569 to 0.00, $\Delta W = 0.025$] (b) Advection term [-0.418 to 0.306, $\Delta Wa = 0.05$] (c) Compression term [-0.068 to 0.043, $\Delta Wc = 0.005$]. Baroclinic term is very small [-0.0125 to 0.0187]

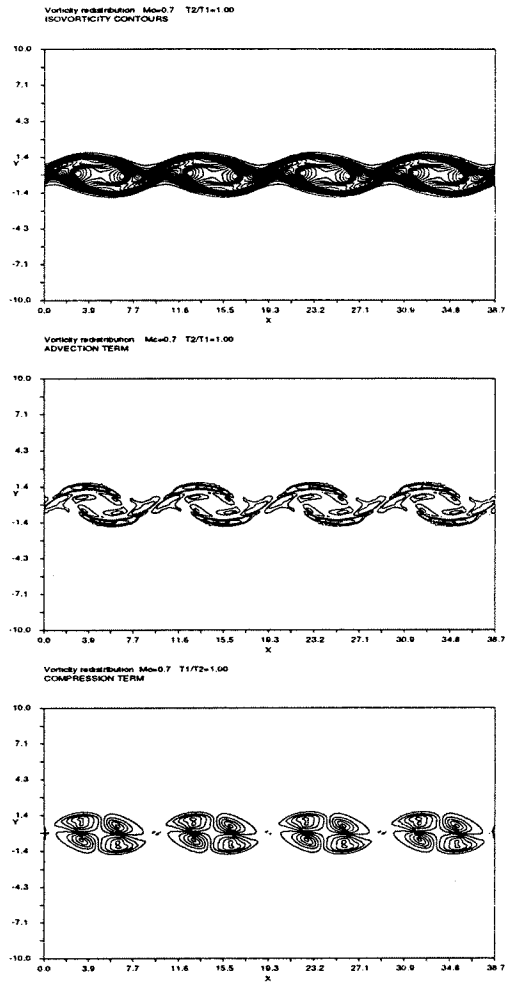

Figure 8: Vorticity field redistribution for $M_c = 0.7$ ($T2/T1 = 1.$). In the panels are illustrated: (a) Vorticity isocontours [-0.839 to 0.00, $\Delta W = 0.05$] (b) Advection term [-0.290 to 0.212, $\Delta Wa = 0.05$] (c) Compression term [-0.344 to 0.132, $\Delta Wc = 0.05$]. Baroclinic term is still small [-0.034 to 0.032].

where U_c is the convective velocity of the large structures, i.e. $U_c = (U_1 a_2 + U_2 a_1)/(a_1 + a_2)$. The most important term causing the vorticity redistribution is the advection term: at low Mach number ($M_c \leq 0.4$) it is much stronger than the dilatational and baroclinic terms. The vorticity is advected into the vortex cores while the braid regions are depleted of it. This is the incompressible redistribution mechanism causing the shear layer instability. The term which describes the change due to the compression of fluid elements is $-\omega_z \vec{\nabla} \cdot \vec{u}$.

With respect to the reference frame moving with speed U_c the mid-braid planes are stationary: the cat's-eye vorticity patterns are fixed and their areas grow in time. The stagnation points correspond to pressure maxima, while the vortex cores correspond to pressure troughs. The fluid particles moving away from the mid-braid region are expanded as they accelerate towards the vortex center ($\vec{\nabla} \cdot \vec{u} > 0$ yields $D\rho/Dt < 0$). Past this point the flow compresses and decelerates towards the other braid region ($\vec{\nabla} \cdot \vec{u} < 0$ yields $D\rho/Dt > 0$). Consequently, the compression term $-\omega_z \vec{\nabla} \cdot \vec{u}$ results negative ahead of the vortex and positive behind it. The expansion and compression cycle has then the effect of increasing the vorticity near the stagnation points and reducing it near the vortex center. This is exactly opposite to the redistribution arising from the advection term. The numerical simulations show that as M_c is increased the vorticity compression effect

becomes comparable in magnitude to the advection term. (figures (7-8)). Therefore the growth rate of the layer is strongly reduced.

The last term in r.h.s. of the equation (7) describes the vorticity change due to baroclinic torque. This is an essentially incompressible effect and arises whenever a density gradient exists across the shear layer. For equal free stream temperatures (which means equal mean densities for a constant thermodynamic pressure) the baroclinic term is an order of magnitude smaller than the other terms. On the other hand, when the densities of the two streams are unequal, during the roll-up the density interface remains sharp in the mid-braid plane and the pressure maximum produces regions with dinamically significant baroclinic torque, i.e. $(\vec{\nabla}\rho \times \vec{\nabla}p)/\rho^2$. As we can see in the figure (9) the baroclinic effect strongly modifies the vorticity distribution. The net circulation of the vortices, however, remains relatively uninfluenced by this redistribution.

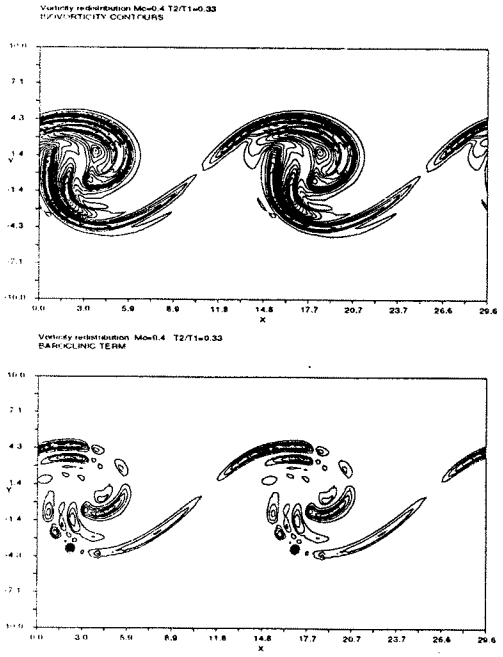

Figure 9: Baroclinic effect for $M_c = 0.4$ when $T2/T1 = 0.33$: (top) the shape of the vortices is strongly modified; (botton) the baroclinic term [-0.537 to 0.381, $\Delta Wc = 0.06$]. is comparable to the advection term and reduces the growth.

Eddy shocklets in the 2-d flow field

For $M_c \geq 0.7$ the flow fields develop eddy shocklets. These shocks remain attached to the vortices and travel with them.

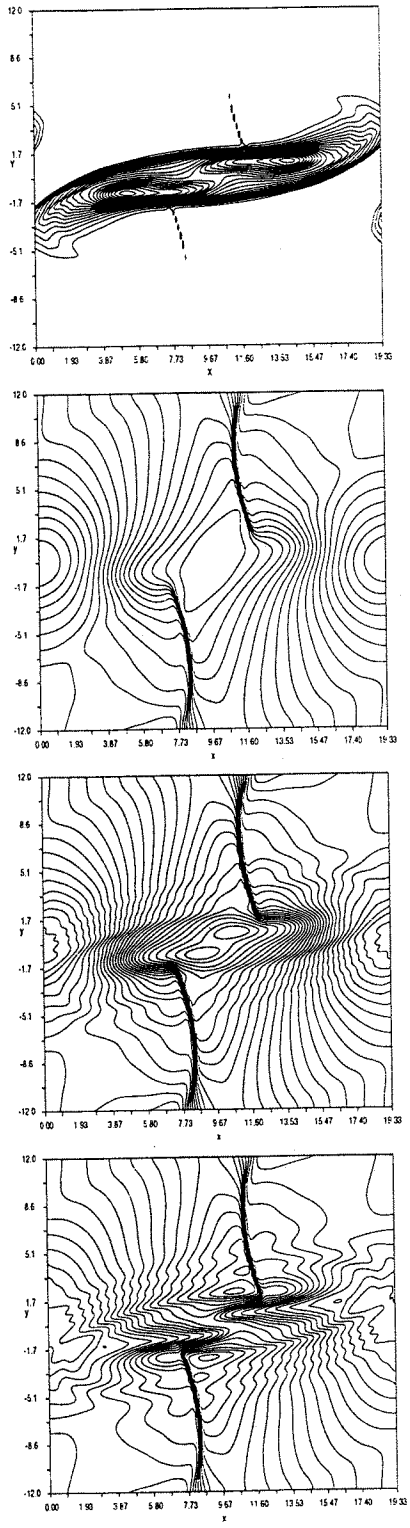

Figure 10: Eddy shocklets into the flow field for $M_c = 0.7$ ($T2/T1 = 1$) during the pairing event.In the panels are plotted isocontours of vorticity, pressure, density and temperature respectively.

For $M_c = 0.7$ the shocks arise during the vortex pairing events, but the flow field is otherwise shock-free. For $M_c = 0.8$ the shocklets are produced during the roll-up. An example of flow fields with eddy shocklets is presented in the figure (10). As observed earlier, the flow accelerates and decelerates around the vortices travelling from a mid-braid region towards the other one. As the convective Mch number is increased, one can observe the presence of local regions near the vortex cores where the relative Mach number of unity is exceeded. This supersonic flow slows down first by going through a shock, becoming subsonic, and then decelerating further by compression towards the stagnation points. The regions of expansion are consequently more spread out and the region of compression more compact (essentially within the eddy shocklet). One can observe that the vorticity increases because of the compression through the shock, as well as the entropy grows. The induced velocity pattern associated with the fluid expansion and compression opposes the entrainment velocity induced by the clumped vorticity field. This may cause a further reduction in the entrainment of fluid into the layer.

References

(1) G.L. Brown & A. Roshko, *On Density Effect and Large Structures in Turbulent Mixing Layers*, J. Fluid. Mech. vol. 64, Pt. 4, 1974, pp. 775-816.

(2) D. Papamoschou & A. Roshko, *The Compressible Turbulent Shear Layer: An Experimental Study*, J. Fluid. Mech. vol. 197, 1988, pp. 453-477.

(3) D. Papamoschou, *Structures of the Compressible Turbulent Shear Layer*, AIAA Paper 89-0126, jan. 1989.

(4) N.D. Sandham & W.C. Reynolds, *Compressible Mixing Layer: Linear Theory and Direct Simulation*, AIAA J., vol. 28, n.4, 1989.

(5) N.D. Sandham & W.C. Reynolds, *Three-dimensional Simulations of Large Eddies in the Compressible Mixing Layer*, J. Fluid. Mech. vol.224, 1991, pp. 133-158.

(6) M.M. Rogers & R.D. Moser, *The Three-dimensional Evolution of a Plane Mixing Layer: the Kelvin-Helhmoltz Rollup*, J. Fluid. Mech. vol. 243, 1992, pp. 183-226.

(7) R.D. Moser & M.M. Rogers, *The Three-dimensional Evolution of a Plane Mixing Layer: Pairing and Transition to Turbulence*, J. Fluid. Mech. vol. 247, 1993, pp. 275-320.

(8) M. Lesieur, P. Compte, J.P. Chollet and P. Le Roy, *Numerical Simulation of Coherent Structures in Free Shear Flows*, Math. Modeling in Combustion, Nijhoff Publishers, 1988.

(9) R. Arina, private communication, 1993

(10) K.W. Thompson, *Time Dependent Boundary Conditions for Hyperbolic Systems.*, J. Comp. Phys. vol. 78, pp. 1-24, 1987

(11) Y. Wada & M.-S. Liou , *A Flux Splitting Scheme With High-Resolution and Robustness for Discontinuities*, NASA TM106452, 1994.

(12) P. Drazin & W. Reid, *Hydrodynamic stability*, Cambridge Univ. Press, 1981.

(13) C. Canuto, M.Y. Hussaini, A. Quarteroni, T.A. Zang, *Spectral Methods in Fluid Dynamics*, Springer-Verlag, 1987.

(14) M.C. Soteriou & A.F. Ghoniem *Effect of the Free Stream Density Ratio on Free and Forced Spatially Developing Shear Layer*, Phys. Fluid. vol. 7, pp. 2037-2051, 1995

(15) S. Lele, *Direct Numerical Simulation of Compressible Free Shear Flows*, AIAA Paper 89-0374, jan. 1989.

(16) M. Lesieur, *Turbulence in Fluids*, Kluwer Academic Publishers, 1993

(17) A.D.D. Craik *Wave interactions and fluid flows* Cambridge University Presse , 1990

(18) J. Chen, B.J. Cantwell, N.N. Mansour, *The Effect of Mach Number on the Stability of Plane Supersonic Wake* Phys. Fluid. A vol. 2 (6), pp. 984-1004, 1990